
Biological Evolution and Genetic Algorithms

Exploring the Space of Abstract Tile Self-Assembly

Christian Schroeder de Witt¹

Abstract

A physically-motivated genetic algorithm (GA) and full enumeration for a tile-based model of self-assembly (JaTAM) is implemented using a graphics processing unit (GPU). We observe performance gains with respect to state-of-the-art implementations on CPU of factor 7.7 for the GA and 2.9 for JaTAM. The correctness of our GA implementation is demonstrated using a test-bed fitness function, and our JaTAM implementation is verified by classifying a well-known search space $S_{2,8}$ based on two tile types. The performance gains achieved allow for the classification of a larger search space $S_{3,8}^{32}$ based on three tile types. The prevalence of structures based on two tile types demonstrates that simple organisms emerge preferably even in complex ecosystems. The modularity of the largest structures found motivates the assumption that to first order, $S_{2,8}$ forms the building blocks of $S_{3,8}$. We conclude that GPUs may play an important role in future studies of evolutionary dynamics.

1. Introduction

1.1. Basic Evolutionary dynamics

The fundamental genetic dynamics of populations of living organisms are constrained by the mechanisms of Darwinian evolution (Dobzhansky, 1973). Modern science motivates the detailed investigation of evolutionary processes, e.g. designing vaccinations often requires the understanding of how pathogens will evolve in the future (Domingo et al., 2001). According to Darwin, the fitness of an individual is a measure of its fecundity, i.e. the ability of its phenotype

to reproduce (Darwin, 2003). The phenotype of an organism is the composite of all of its observable traits (Hartl & Clark, 2007). Neglecting environmental influences, all information about a phenotype is encoded in the corresponding genome, or genotype (Hartl & Clark, 2007). Evolution may be understood as the process of adaptation of a population to peaks on a high-dimensional fitness landscape (Wright, 1932; Gavrillets, 1997).

Whether adaptation occurs is governed by the ratio of exploration to exploitation exerted by the biological operators driving the traversal of the fitness landscape: Exploration arises due to random mutation and recombination of genomic information, exploitation through natural selection. If exploitation dominates, disconnected peaks may never be discovered. If, however, exploration dominates, the trajectory through the fitness landscape resembles a random search, unable to adapt to localised features (M.A.Nowak, 2006). Many fitness landscapes only allow adaptation below a critical mutation rate, called the error threshold (M.A.Nowak, 2006). The evolution of an individual genotype, rather than a whole population, may be characterised by the accessibility of its immediate fitness landscape neighbourhood through mutation.

To this end, we define robustness to be the proportion of single mutations that don't change phenotype, and evolvability to be the number of different phenotypes accessible under a single mutation (Wagner, 2008). In conclusion, the key results of genetic dynamics are encoded in the topology of the underlying fitness landscape (M.A.Nowak, 2006). Therefore, identifying a reasonable genotype→phenotype map is essential. We now investigate such a map based on the dynamics of molecular self-assembly which is suitable for the description of the assembling protein quaternary structures, such as the shell of a virus (Johnston, 2010).

1.2. Johnston's Tile Assembly Model

A ubiquitous way by which complex physical structures emerge is through the self-assembly of simple subunits (Whitesides & Grzybowski, 2002). For example, protein subunits assemble into the required quaternary structures for a particular function. Knowing how biology evolves the rule sets to self-assemble structures is therefore crucial

¹Department of Engineering, University of Oxford, Oxford, UK. Correspondence to: Christian Schroeder de Witt <schroederwitt@gmail.com>.

This article is a reproduction of "Biological Evolution and Genetic Algorithms", MPhys Thesis, Christian A. Schroeder, 2012, University of Oxford. Supervisors: Prof. Ard Louis, Dr. Iain Johnston. This thesis was awarded the 2012 Oxford University Tessella Prize for Innovation in Software.

to understand the evolution of simple organisms, such as viruses (Domingo et al., 2001). Self-assembly processes are difficult to observe experimentally due to its short length and time scales, therefore computational simulation may be an important source of insight (Johnston, 2010).

The computational intractability and incomplete knowledge of many atomistic details motivates the development of coarsegrained models of self-assembly which attempt to capture the essential physics while retaining tractability (Johnston, 2010). Johnston (2010) suggest an abstract model of self-assembly based on work by Winfree et al (Rothemund & Winfree, 2000). This model, which we from now on refer to as JaTAM, exhibits rich phenotypic phenomenology and therefore promises to capture a lot of characteristics of general self-assembly processes (Johnston, 2010). These characteristics include the correlation between decreasing occurrence frequency with increasing structural complexity found in natural proteins, as well as the mutability of assembled structures (Ahnert et al., 2009).

The model's building blocks consist of squares with labelled edges which are assembled on a planar grid according to fixed interaction rules. Squares are chosen from an inexhaustible library of tile types called a tile set, of which the first tile is placed first in the assembly process. Interaction rules state that labels bind in pairs, i.e. $1 \leftrightarrow 2$, $3 \leftrightarrow 4$ etc. except for label 0, which is generally inert. Non-bonding label combinations neither repel nor attract. Binding is thermodynamically irreversible, which is reasonable if thermodynamic noise is much smaller than interaction strengths between subunits.

Tiles may be rotated orthogonally, but not flipped. The particular choice of interaction matrix differs from Winfree's original model and results in a higher ratio of structures exhibiting dihedral, instead of rotational, symmetry (Johnston, 2010). Assembly proceeds by stochastically adding bonding tiles to the existing structure until either no further tiles can be assembled, or the resulting structure hits the edges of the assembly grid.

If a tile set is not guaranteed to always assemble to a unique grid configuration it is denoted non-deterministic. Trivial non-determinism occurs if at any step, more than one tile can be selected to bond to the same bonding site. More subtly, Steric non-determinism may arise if two assembly "arms" converge at variable speeds (see Figure 1).

Self-assembly can be cast in a formal mathematical language, which has previously been used to e.g. prove its Turing completeness (Doty et al., 2012). For details see Appendix B.1.

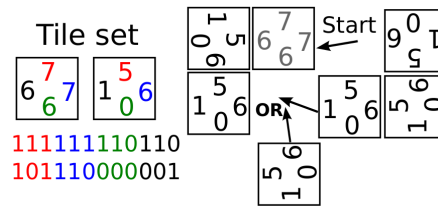


Figure 1. An example tile set that exhibits steric non-determinism, i.e. the final structure depends on the order in which tiles are assembled during the assembly process. The binary string represents a simple binary encoding of the tile set information.

1.3. The benefits of GPUs

A graphics processing unit (GPU) is an electronic device designed for high-throughput parallel computation at low power consumption compared to CPU clusters (NVidia, 2012a). Central Processing Units (CPUs) feature a small number of processing cores and a large, shared low-latency cache facilitating sequential operation. In contrast, Graphics Processing Units (GPUs) feature a large number of processing cores with comparatively tiny low-latency caches, called shared memory, and are designed for large dataparallel throughput. Nvidia®, a leading GPU manufacturer, recently announced to get involved in the development of CPUs (Dally, 2011). This suggests that future hardware architectures will feature intimate interaction between GPUs and CPUs and therefore software will need to exploit the benefits of both.

The increasing need for high-throughput computing in science (NVidia, 2012a), has established the use of GPUs in a number of disciplines within bioinformatics, e.g. sequence alignment (Schatz et al., 2007). In order to benefit from GPUs, a given algorithm needs to be efficiently parallelisable (NVidia, 2012a). In these cases, the performance gains achieved compared to execution on modern CPUs are usually on the order of one to two magnitudes (NVidia, 2012a).

The scope of current simulations of evolutionary dynamics performed by Johnston et al, including JaTAM, is greatly limited by a lack of computational performance (Johnston, 2010). The achievement of significant performance gains for example permits the increase of population sizes in adaptation simulations, thus lowering error bars on simulation properties such as mean fitness. Furthermore, it makes feasible the detailed classification of self-assembled structures emerging from more than two tile types, which allows the exhaustive study of evolvability and robustness in more complex ecosystems. Both these aspects may be required to improve the understanding of e.g. virus evolution (Domingo et al., 2001).

In this paper, we, for the first time, aim to study a significant subset of all self-assembled JaTAM structures formed from

three tile types. To this aim, we first specify how the tile sets assembling into phenotypes are encoded in the respective genomes. We then describe a class of heuristic algorithms commonly used for the study of evolutionary dynamics of finite population sizes. Observing that these algorithms are efficiently parallelisable, we proceed by implementing them on GPU. Before finally classifying a subset of all self-assembled JaTAM structures formed from three tile types, we reproduce some known results to assert the functionality of our implementation.

2. Implementation on GPU

2.1. Binary encodings

To computationally simulate JaTAM, one needs to somehow encode its rule sets in binary strings such that realistic biological operators may be defined. As interaction rules are binary by nature, they can simply be encoded in a binary matrix. Keeping interaction rules constant in time, all relevant phenotypic information is encoded in the tile set. Therefore, each binary encoded tile set constitutes one genome and the combinatorial freedom of the respective bitstring constitutes the genome search space $S_{a,b}$, where we define a to denote the number of tile types and b the number of bonding labels of the underlying JaTAM assembly.

Tile sets may be encoded by sequentially encoding the edge labels of subsequent tiles from the tile set into a binary string, as shown in Figure 1. If the number of different bonding labels is a power of 2, a single genomic mutation may be defined to consist of a single bit flip in the respective bit string (Johnston, 2010). For a formal justification of the binary encoding chosen for this paper, see Appendix B.3. We proceed by investigating a computational algorithm which is extensively used to simulate the evolutionary dynamics of binary encoded bitstrings (Holland, 1992b).

2.2. Genetic Algorithms

Genetic Algorithms (GAs) are a class of probabilistic search heuristics which enhance a purely random exploration by the ability to exploit local correlations in search space. This compromise between exploration and exploitation is efficient in locating extrema on a rugged fitness landscape (Holland, 1992b). GAs are therefore commonly used in problems involving complex, highdimensional fitness landscapes, from job and process scheduling and gaming strategy (Kumar et al., 2010) to antenna design (Linden et al., 2004).

Natural selection is modelled on the basis that the probability of a genome to be selected is proportional to the normalised fitness value of that genome. A simple selection mechanism which guarantees the above is global roulette wheel selection with normalised weights $F_i \in \{\mathbb{R}, F_i \geq 0\}$

(Johnston et al., 2011, Appendix A). $F_i = \mathcal{N}f_i$, where f_i is the fitness value assigned to the i th genome and $\mathcal{N}^{-1} = \sum_i f_i$. Roulette wheel selection is equivalent to randomly throwing darts on a dartboard sub-divided into normalised areas of size proportional to the attached weights. The selected individual is the one in whose area the dart lands. Random single-point mutation is modeled as an independent Poisson process of mean mutation rate μ for each gene. As far as Johnston's model is concerned, μ is defined to be uniform across genomes and constant in time. The effect of mechanism-dependent mutation rates may be investigated by further research.

A simple way to characterise the parametrisation of a given GA with respect to the underlying search space are the concepts of adaptation time and discovery time (Holland, 1992a). Adaptation time measures the mean number of generations until a proportion x of the population lies within a given fitness interval. Discovery time denotes the mean number of generations until a specific phenotype or fitness value has been encountered for the first time. Both these concepts need to be defined with respect to well-defined initial conditions (Mitchell, 1998)

2.3. CUDA architecture

Programming on General-purpose Graphics Processing Units (GPGPUs) has recently been facilitated by the introduction of novel parallel-computing frameworks, such as Nvidia's Compute Unified Device Architecture (CUDA) (NVidia, 2012d) and Khronos Groups' Open Computing Language (OpenCL) (Group, 2012).

The Nvidia CUDA environment (see Figure 2.3) is an abstraction layer on top of GPU hardware architecture (NVidia, 2012d). CUDA-code is divided into host code, which resides on CPU caches, and device code, which is pre-cached on GPU. The device consists of the graphics card, the host consists of the rest of the hardware (namely the CPU). Data transfer between host and device is low compared to device throughput. A kernel is the GPU equivalent of a CPU process. Device memory must be allocated by the host prior to a kernel launch. At the end of a simulation, results must be copied back from GPU to CPU. The kernel launch topology is divided into three-dimensional grids of blocks and threads whose dimensions are fixed for the duration of a kernel launch.

A block may contain up to 1024 threads, which each execute an instance of the same kernel. Adjacent threads within a block are sub-divided into packages of 32, each constituting a warp. Each thread may, to first order, be seen to represent a single process on an independent processing unit. There are limits to this picture, however: threads within a single warp are executed at lockstep, i.e. if a single thread enters a

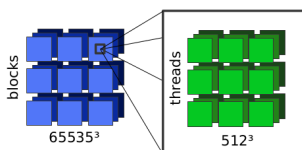


Figure 2. CUDA kernel launch topology

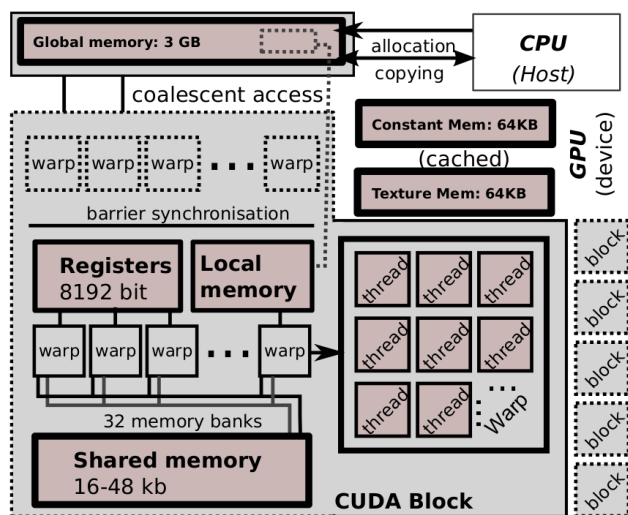


Figure 3. A graphical overview of NVIDIA CUDA architecture. Notice the complex memory hierarchy.

code branch, all other threads in the same warp have to wait until it has left the branch again.

All threads within a block may be forced to wait for each other at a particular code segment by the use of an in-built barrier synchronisation function (see Figure 2). This is useful if a code segment relies upon the fact that all threads have terminated the previous segment. All threads within a block share a small region of low-latency shared memory and a set of fast registers. All threads of all blocks share a large region of high-latency global device memory (see Figure 2).

Safe simultaneous write accesses of multiple threads to shared memory resources may be performed using atomic operations. These are in-built routines which prevent "race" conditions where the read-write cycles of multiple threads are randomly mingled by the hardware, producing an undefined outcome. Trying to synchronize threads belonging to different blocks via atomic operations poses the threat of deadlocks, i.e. that all threads wait for each other to free a particular resource. We observe that this form of global synchronization is most efficiently achieved by exploiting the fact that all threads of a kernel will be synchronized just before the kernel terminates (NVidia, 2012d).

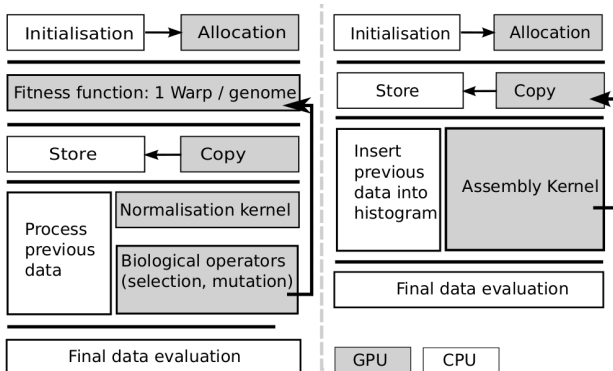


Figure 4. Process layout for a model genetic algorithm with a self-assembly fitness function (on the right). Process layout for the classification of JaTAM structures (on the left).

3. Choice of Development Tools

We choose to work with python as the host language and, for performance reasons, CUDA C on device side. A templating language called Jinja2 [BSD12] serves as a host-based metaprogramming-language, which allows the runtime generation and calibration of kernel code. The CUDA C compiler, nvcc, currently supports only a subset of the C++ specification. We choose to avoid recursion, function pointers and classes for downward compatibility reasons with older GPU architectures (NVidia, 2012d). Instead, we use structs for object-oriented kernel design.

For debugging purposes, we use cuda-gdb, a Nvidia variant of the GNU Debugger (NVidia, 2012d). As a random number supply, we employ the XORWOW-generator from Nvidia's CURAND-library (NVidia, 2012c). This generator is similar in quality to the commonly-used Mersenne twister (Matsumoto & Nishimura, 1998). CURAND may be used with PyCUDA if name-mangling of the C++ compiler is suppressed (see Appendix E.1). Unrolling for-loops may result in significant performance gains (Murthy et al., 2010).

We also observe that thread synchronization within for-loops is sometimes unreliable. We thus use Jinja2 to unroll loops at runtime (see Appendix E.2).

3.1. Parallelising Johnston's GA

The execution of general-purpose GAs on GPUs has shown to be especially efficient using a "parallel island" model (Pospichal et al., 2010). For the scope of this paper, it is sufficient to notice that this approach by design suffers from data inconsistencies and physically unintuitive selection operators (see Section 3.1), which is acceptable for general optimisation problems, but limits its use within theoretical biology. At the expense of performance, We therefore adapt the model to our needs. We assign one thread to each genome performing the required biological operators. In

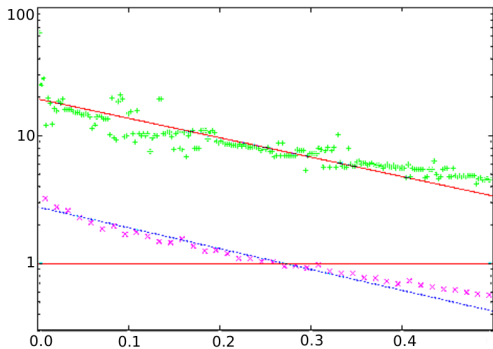


Figure 5. Performance ratio for bitwise mutation / mutation by distribution vs. mutation rate μL .

contrast to (Pospichal et al., 2010), we demand synchronisation between all threads of all block after each generational step in order to preserve data consistency. We also introduce global roulette wheel selection both for sexual and asexual reproduction, instead of the local selection model proposed by (Pospichal et al., 2010).

To this goal, the normalisation constant N is determined using a separate summation kernel (see Figure 4). The roulette wheel selection is then performed from constant device memory which is optimised for memory access patterns that are similar for all threads within the same warp (NVidia, 2012d).

True bit-encoding of genome information is significantly more performant than representation by boolean values (Pedemonte et al., 2011). Therefore, we designed efficient bit-wise implementations for mutation, single-point and uniform crossover operators. Importantly, mutation from Poisson distribution proves significantly faster than conventional bit-by-bit flipping in the small μL regime. This means we first randomly choose the number of bits to be flipped and subsequently choose the sites where they should be flipped. The number of bits to be flipped k follows a Poisson process with mean λ and probability distribution:

$$p(k) = \frac{\lambda^k e^{-\lambda}}{k!} \quad (1)$$

A bitmask is used to avoid multiple flipping at the same sites but may, for $\mu L \ll 1$, be omitted. Figure 5 below demonstrates a significant speed-up even at small genome bytelengths for $\mu L \leq 0.5$. The graph on top corresponds to a genome length of 128 bytes, the lower graph to a length of 3 bytes. 105 iterations using a single CPU thread were performed for each data point. For large genome bytelengths, mutation from distribution is several orders of magnitude faster than bit-wise flipping. For our efficient bit-wise implementations of common evolutionary operators see appendices D, D.1.

3.2. Parallelising JaTAM

We choose to assemble 32 tile sets per block, scheduling 8 threads from adjacent warps per assembly. This allows us to store the grid for each assembly within a single shared memory bank, enabling an efficient shared memory access pattern called bank-conflict free access (NVidia, 2012b). Ensuring that assembly threads are from different warps allows the usage of atomic operations within each assembly process - atomic operations among threads of the same warps result in undefined behaviour as these threads execute at lockstep (NVidia, 2012d). Grid initialisation is performed by all the threads in an assembly process in parallel. This compensates for shared memory access latency.

For the polyomino-assembly fitness function, we a single-threaded movelist-based algorithm offered by Johnston, which stochastically grazes through the assembly frontier on a finite grid of dimension d (Johnston, 2010). This implies that 7 of the 8 assembly threads are idle during assembly. Each position on the assembly frontier is isotropically checked for ambiguous bonding situations and in this case, the structure is classified nondeterministic. This checks for trivial and first-order steric non-determinism at the same time and we therefore do not distinguish between the two. Higher-order steric non-determinancy is stochastically detected by detailed comparison of k independent assembly processes. See Appendix 2 for a flow chart of the movelist assembly process.

To optimise the assembly process, each bonding label is pre-assigned a list of tiles and their orientations which bond to it. In order to only detect phenotypic nondeterminancy, we remark that this list needs to be further processed in order to eliminate double tile types and symmetric tiles. Also, steric non-determinism detection should be conducted only after the assembly has terminated to allow rotational invariance of assembled shapes - this could be included straightforwardly, but we prefer to be consistent with Johnston et al. (2011).

As shared memory features no heap for dynamic memory allocation, we choose to implement the movelist as a combination of a pre-allocated *Last-In-First-Out (LIFO)*- stack and grid markings (see below). This implies a higher degree of locality in assembly frontier traversal compared to random traversal using dynamic lists and reduces the need for pre-allocated storage space by about 5. We, however, observe that the detection of steric non-determinism is not significantly affected by localised traversal as movelist elements are added to the stack in random order.

3.3. Classifying self-assembled shapes

Grid-wise comparisons of assembly structures as employed by Johnston are unsuitable for the classification of larger search spaces than $S_{2,8}$ as they are resourceexpensive and

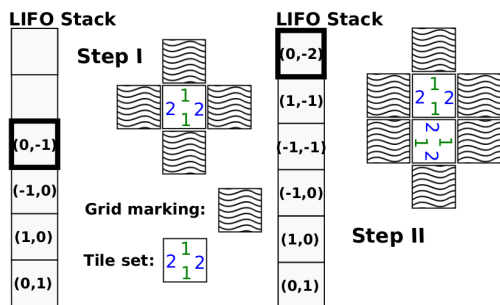


Figure 6. Illustration of an assembly process using both grid markings and a LIFO-stack. Note that elements are randomly inserted and removed from the top, therefore, growth exhibits a large degree of spatial locality.

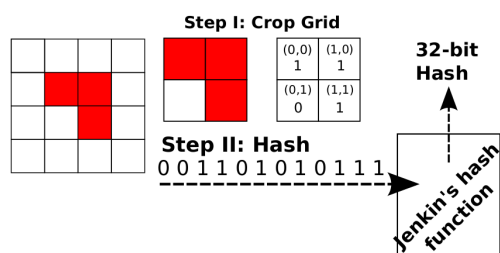


Figure 7. An illustration of grid hashing.

ambiguous in higher search spaces (Johnston, 2010). As the register manipulation of composite data types in CUDA is tedious, I employ a 32-bit *one-at-a-time hash* (Jenkins, 1997). Each phenotype shape is hashed by subsequently encoding the positions of all occupied grid sites relative to the coordinates of an assembly grid cropped to the phenotype shape. Cropping is readily parallelisable using atomic operations (see Appendix F.6). For an expected number of 1000 different phenotypes, the probability that at least one hash collision occurs is

$$1 - \prod_{i=0}^{1000} (1 - i \cdot 2^{-32}) \approx 0.01\%. \quad (2)$$

Therefore, a 32-bit hash is sufficient for the purpose of this paper. We note that hashes may be made rotationally invariant if one chooses to hash each grid for all four orthogonal rotations individually, sorts these hashes by e.g. numerically and sequentially hashes them again with Jenkin's hash function.

3.4. Exploiting CPU and GPU concurrently

Classifying a genome search space consists of assembling each tile set, hashing the resulting structure and inserting it into a histogram counting the occurrences of each hash. As GPUs have a finite global memory size, on a Tesla C2050,

only about 2^{16} assembly grids of dimension 19×19 may be stored at any one time. For searchspace classification, this requires execution in batches.

However, the execution may be asynchronous: While the GPU executes one batch, the previous batch is meanwhile sorted on CPU (see Figure 4). For our model, this was shown to efficiently hide CPU processing times. Alternatively, one may just copy the hashes from GPU and the bitstrings for the respective tile sets assembling to those hashes. After having created the histogram on CPU, one may just re-assign assembled structures to hashes by considering the structure which predominantly assembles from the respective tile set.

4. Results

All CPU timing references were measured by Johnston (Johnston, 2010) on an Intel® Core™ i5- 2520M CPU running at 2.50GHz and sufficient RAM. GPU timings were measured on a single NVidia Tesla C2050 card. Both these devices represent state-of-the-art technology.

4.1. Classification of $S_{2,8}$

To verify the correctness of the polyomino assembly routine, I re-classify the search space $S_{2,8}$. Comparing results to Johnston's yields identical values for the occurrence of deterministic structures (see Figure 8). There is evidence that the mis-classification of non-deterministic structures as deterministic structures can be made arbitrarily small with increasing k (see Figure 8). The only phenotype shape with both deterministic and sterically non-deterministic rulesets is found to be the 12-mer (see Figure 8).

Structures of steric non-determinism outweigh unbound structures by a factor of ≈ 2.2 . This suggests to optimise our assembly algorithm for steric non-determinism detection in the future, which may be achieved by conducting as many assembly processes in parallel at any one time. Finally, a speedup of a factor 2.9, as compared to Johnston, was detected for our CPU/GPU hybrid implementation.

4.2. Genetic algorithms on a Fujiyama landscape

To demonstrate the flawlessness of our implementation, we implement our genetic algorithm on a test-bed fitness landscape referred to as 'Fujiyama'-landscape. This landscape consists of a single, broad peak. In evolutionary dynamics, the study of adaptation behaviour on Fujiyama landscapes is insightful as locally, any smooth fitness function may be approximated by a single peak. In simple binary encoding, a suitable fitness function consists of the Hamming weight $H(x)$ of a genome x , which is equivalent to the number of set bits in the respective bitstring. We choose to investigate the adaptation and discovery times for a population size of

512.

Each data point in Figure 10 represents the median of 100 independent simulations. A simulational cutoff at 20000 generations is employed. Error bars were derived from bootstrapping with sample size 100 and 104 repetitions. I find discovery times to power-law decrease with increasing mutation rate, and the existence of a catastrophic adaptation cut-off in the vicinity of $\mu L = 1$. Both these results are fundamental characteristics of genetic algorithms (Johnston, 2010). A speed-up of our implementation of factor 7.7, as compared to Johnston, was measured.

4.3. Classification of a subset $S_{3,8}^{32}$ of $S_{3,8}$

Whereas there exists a large amount of literature on the study of individual search spaces (Johnston, 2010), this is currently not the case for the comparison between different search spaces. Using our CPU/GPU hybrid implementation of JaTAM and a process layout given in Figure 4, we therefore for the first time classify a search space which may be expected to yield phenomenology distinct from $S_{2,8}$. The JaTAM search space for 3 tile types and 8 distinct bonding labels is 4096-times larger than $S_{2,8}$ and its classification is expected to yield a rich amount of shape phenomenology.

We provide a GPU classification of the first 32 bits (thus a 16th) of this search space, which means that the seed tile type and second tile type may have arbitrary bonding labels, while the third tile type is fixed to bonding labels $\{x_1, x_2, y, 0\}$, where $x_1, x_2 \in [0, 7]$ and $y \in \{2, 4, 6\}$. A frequency classification of deterministic structures shows that the deterministic structures of $S_{2,8}$ are the most frequent ones in $S_{3,8}^{32}$.

This is expected, as the probability that the third tile does not interact with the other two tiles is increased due to the fixed zero bonding site. The frequency differences of certain flipped forms is caused by the fact that these would require tile three to flip bonding labels, which is only possible if $x_2 = 0$ or $y = x_1$.

The most frequently encountered structures in $S_{3,8}$ are in fact the simple structures found in $S_{2,8}$. This indicates that simple structures continue to be common in complex ecosystems. Furthermore, the largest structures formed exhibit striking modularity: Most of them consist out of trivially-assembled copies of members of $S_{2,8}$. This motivates the assumption that to first order, $S_{2,8}$ forms the building blocks of $S_{3,8}$. An overview of all 361 deterministic structures encountered in $S_{3,8}$ can be found in Appendix A.

5. GPU: Pitfalls, Performance Gains and Coding Standards

5.1. Pitfalls

Langdon advised in 2011 that scientists should refrain from writing new pieces of software using CUDA whenever possible because of the frequent appearance of bugs that were hard or almost impossible to debug (Langdon, 2011). As this project featured rather complex kernels (up to 1706 lines for JaTAM classification, which is at least 17- times larger than typical kernel sizes according to Langdon (Langdon, 2011)), virtually all of the pitfalls reported by Langdon were encountered. Some of these resulted in intraceable bugs and lead three times to a complete redesign of our source code methodology.

On top of Langdon's observations, compiler errors generated by the CUDA compiler `nvcc` were often highly misleading (if it hadn't crashed during compilation). Tracebacks of `cuda-gdb` often merely featured unresolved memory addresses and `printf` functions were prone to buffer overflows, thus making debugging frequently unfeasible and turning the graphics card into an effective "black box".

In response, we developed a coding model and compatibility layer that allowed us to first develop and debug our multi-threaded kernel code on CPU. Then, we performed minor modifications to port the code to GPU architecture. This approach in principle also allows easy performance comparisons to implementations on multi-threaded CPUs.

5.2. Opportunities for further code optimisation

The complexities of code development made it impossible to include some important optimisation features in the current version of our implementation. This may explain why the performance gains achieved for the GA are not as large as may have been expected from the literature (Pospichal et al., 2010). Most notably, our current JaTAM classification spends 83% of its time on assembly grid initialisation. We suggest that this time may be reduced by keeping track of the positions were tiles have been assembled and only re-initialising these. A

Additionally, we found that grid initialisation times could be reduced up to 4-fold by increasing memory access granularity through the use of pointer re-interpretation (see Appendix D.2). Time spent assembling the structures themselves may be reduced using a parallel assembly process, which may either involve a pure random pick in-place assembly routine (see the flowchart in Appendix 1) or a hybrid approach featuring either separate or shared movelists for each assembly thread (see Appendix F.5 for a push function of a multi-threading safe LIFO stack).

We conclude that even our only modestly optimised GPU

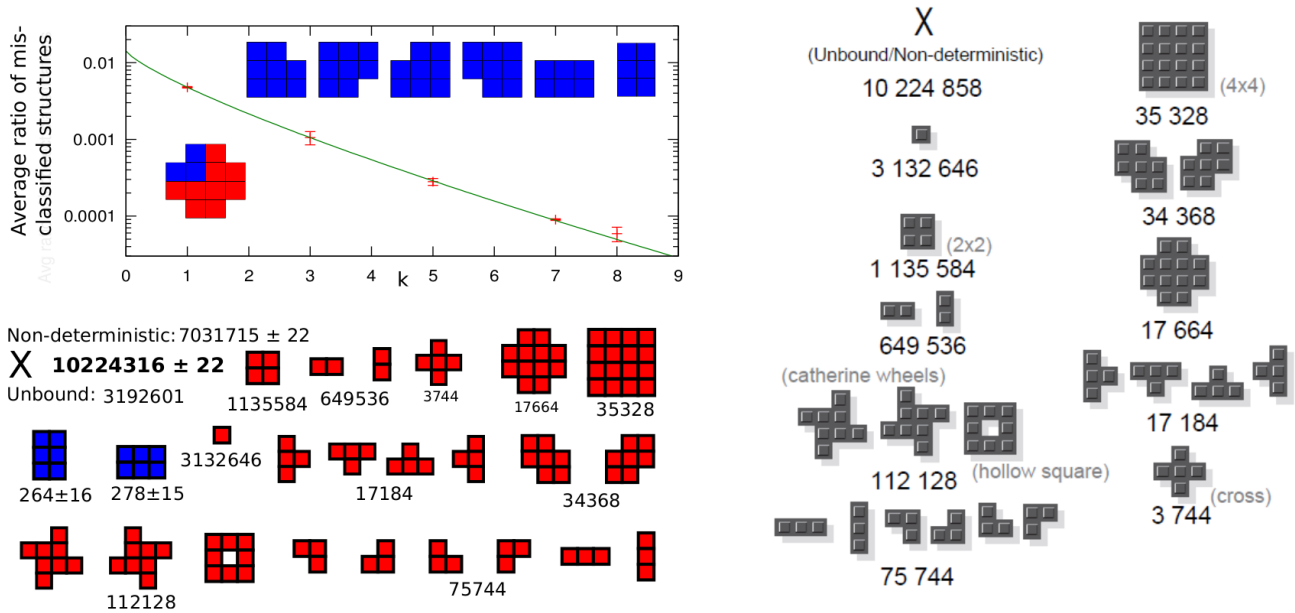


Figure 8. Right: Johnston's enumeration of $S_{2,8}$. Upper left: Ratio of mis-classified structures with k . Lower left: GPU classification of $S_{2,8}$ at $k = 8$.

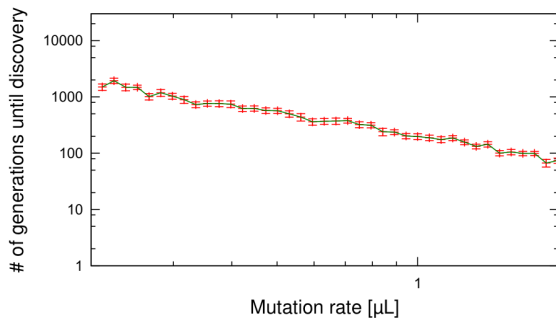


Figure 9. Discovery times for $H = 25$ on Fujiyama landscape (Johnston, 2010).

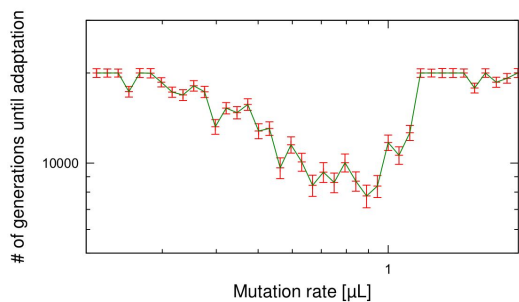


Figure 10. Adaptation times for half of the population to be at $H > 25$ on Fujiyama landscape

implementations yield significant performance gains compared to state-of-the-art CPU implementations. These performance gains may be further increased by performing further optimisation measures as suggested. This indicates that GPUs are likely to have a prominent future in the study of genetic population dynamics.

5.3. Coding standards in the sciences

The difficulties encountered in the development of our GPU implementation immediately raise the question whether it is possible to avoid many common pitfalls by employing state-of-the-art coding standards from within the computer science community. We come up with the following suggestions: Software written in imperative programming languages should be designed from flow-charts (procedural) and/or UML activity diagrams [see App. C] (object-oriented) level. These charts should be supplied for peer-review and enable flow-level analysis.

The source code of unit tests (see Appendix C) and their results should be supplied for peer-review as well to complement flow-level analysis. Domain-specific languages (DSLs) are special-purpose programming languages designed for usage in particular problem domains. Usage of these may abstract away many possible error sources. Creating a new DSL, however, is comparable to writing a compiler and thus difficult and error-prone (Cartney, 2012). An example of a system that allows the creation of new DSLs is Cartneys recent work (Cartney, 2012). Functional programming languages allow for an abstract flow-independent

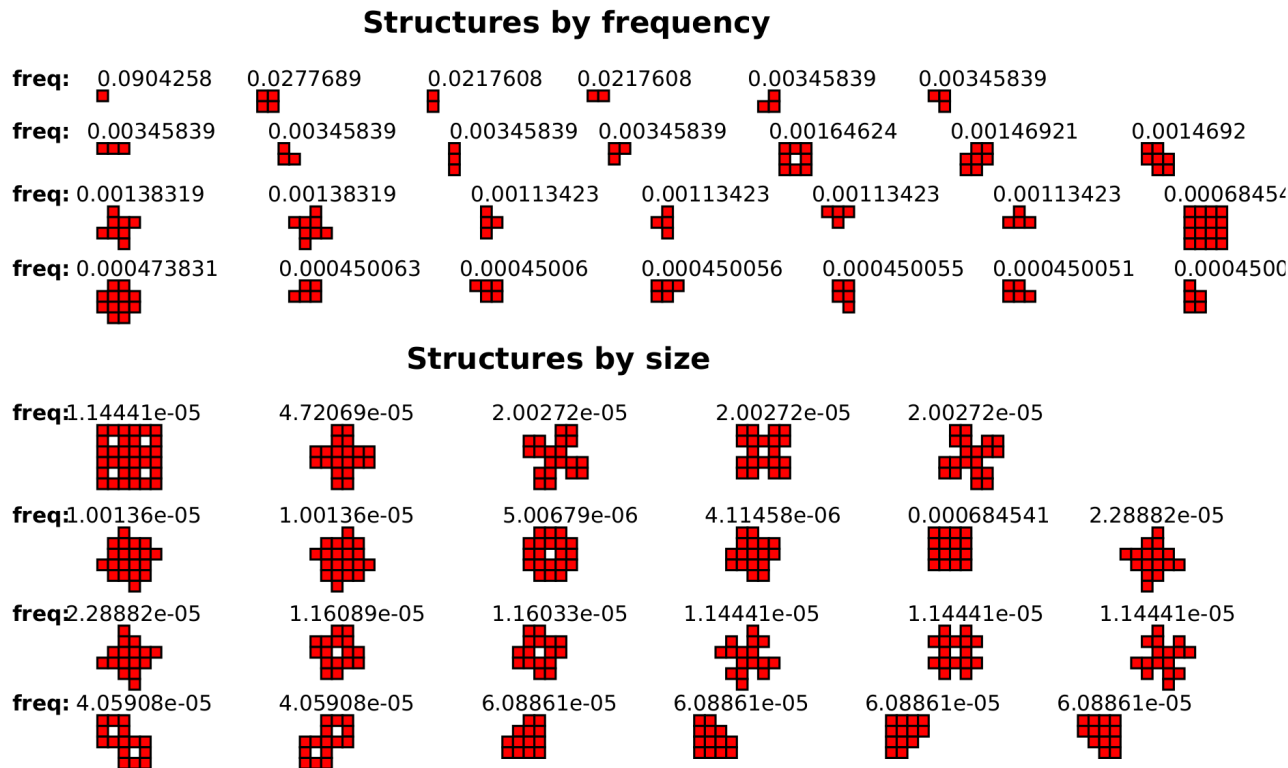


Figure 11. Selected phenotype shapes from the classification of $S_{3,8}^{32}$ at $k = 7$. For a full list, see Appendix A

problem formulation, often resulting in smaller code sizes as well. There exists a large infrastructure of quantitative unit testing tools such as QuickCheck. Equational reasoning allows for fine-grained formal verification in some circumstances (Harper, 2012). Problems that are efficiently parallelisable should be expressed in a concurrent programming language.

While a number of concurrent imperative languages are under development, such as python/copperhead (copperhead, 2012), functional programming languages arguably embody parallelism more naturally (Chakravarty, 2009). The functional programming language Haskell offers industry-grade extensions for data-parallel programming (Wu, 2012; GHC, 2012). Computer scientists are currently developing functional programming language derivatives, such as Accelerate (Chakravarty et al., 2011), which are compiled to CUDA C or Parallel Thread eXecution (Nvidia, 2007) code and thus produce code for later execution on GPUs.

We conclude that future researchers in the sciences may especially benefit from learning concurrent, as well as functional, programming languages. For performance reasons, we, for this project, chose to program in CUDA C and Python, which are both imperative languages.

6. Conclusion and Outlook

We implemented a biologically-inspired evolutionary model on a graphics card. This resulted in a performance gain of factor 7.7 over state-of-the-art implementations. The correctness of our implementation was demonstrated on a Fujiyama fitness landscape. We developed a novel mutation algorithm in the process which significantly outperformed conventional algorithms at low mutation rates.

Additionally, a two-dimensional model of self-assembly was implemented using a CPU/GPU hybrid model. This resulted in a performance gain of factor 2.9 over state-of-the-art implementations. The correctness of our implementation was demonstrated by classifying a well-known search space named $S_{2,8}$. A universal method of classifying self-assembled shapes using hashing was introduced. We list additional optimisation measures which may result in further significant performance gains in the future.

Using our CPU/GPU hybrid implementation, a subset of a previously unstudied self-assembly search space named $S_{3,8}$ was classified. It is found that this search space prevalently contains simple structures, which indicates that simple organisms preferably emerge even in complex ecosystems. The modularity of the largest structures found motivates the assumption that to first order, $S_{2,8}$ forms the building

blocks of $S_{3,8}$. Our work may easily be extended to study evolvability and robustness in $S_{3,8}$.

Finally, on the basis of this project, we discuss the challenges that novel hardware architecture poses to traditional coding standards in the sciences and what technologies may be taught to future students in the sciences in order to increase the tractability of their code.

We conclude that GPUs may have significant applications in future studies of evolutionary dynamics in theoretical condensed matter physics.

References

- Ahnert, S. E., Johnston, I., Fink, M., Doye, J., and Louis, A. Self-assembly, modularity and physical complexity. *Phys. Rev. E*, 2009.
- Cartney, L. Generating GPU code from domain specific languages, February 2012.
- Chakravarty, M. General purpose GPU computing @ programming languages & systems, 2009. URL <http://www.cse.unsw.edu.au/~pls/cuda-workshop09/slides/gpu-research.pdf>.
- Chakravarty, M., Keller, G., Lee, S., McDonell, T., and Grover, V. Accelerating haskell array codes with multi-core GPUs. *Declarative Aspects of Multicore Programming (DAMP 2011)*, 2011.
- copperhead. copperhead - data parallel python. <http://code.google.com/p/copperhead/>, 2012. URL <http://code.google.com/p/copperhead/>.
- Dally, B. "Project denver" processor to usher in new era of computing. <http://blogs.nvidia.com/2011/01/project-denver-processor-to-usher-in-new-era-of-computing/>, January 2011. URL <http://blogs.nvidia.com/2011/01/project-denver-processor-to-usher-in-new-era-of-computing/>.
- Darwin, C. *Origin of Species*. Signet Classic, 2003.
- Dobzhansky, T. Nothing in biology makes sense except in the light of evolution. *The American Biology Teacher*, 35: 125–129, March 1973.
- Domingo, E., Holland, J. J., and Biebricher, C. K. *Quasispecies and Rna Virus Evolution: Principles and Consequences*. R G Landes Co, Georgetown, Tex. : Austin, Tex, March 2001. ISBN 978-1-58706-010-6.
- Doty, D., Lutz, J. H., Patitz, M. J., Schweller, R. T., Summers, S. M., and Woods, D. The Tile Assembly Model is Intrinsically Universal. pp. 302–310. IEEE Computer Society, October 2012. ISBN 978-1-4673-4383-1. doi: 10.1109/FOCS.2012.76. URL <https://www.computer.org/csdl/proceedings-article/focs/2012/4874a302/12OmNyuPKTx>. ISSN: 0272-5428.
- Gavrilets, S. Evolution and speciation on holey adaptive landscapes. *Trends in Ecology & Evolution*, 12(8):307–312, August 1997. ISSN 0169-5347. doi: 10.1016/S0169-5347(97)01098-7. URL <https://www.sciencedirect.com/science/article/pii/S0169534797010987>.
- GHC. Data-Parallel haskell, 2012. URL http://www.haskell.org/haskellwiki/GHC/Data_Parallel_Haskell.
- Group, K. OpenCL - the open standard for parallel programming of heterogeneous systems, March 2012. URL <http://www.khronos.org/opencl/>.
- Harper, T. Interview on software verification, January 2012.
- Hartl, D. and Clark, A. *Principles of Population Genetics*. Sinauer Associates, Inc. Publishers, Sunderland, MA, 4th edition, 2007. ISBN 978-0-878-93308-2.
- Holland, J. *Adaptation in natural and artificial systems*. MIT press Cambridge, MA, 1992a.
- Holland, J. H. Genetic Algorithms. *Scientific American*, 267 (1):66–73, 1992b. ISSN 0036-8733. URL <https://www.jstor.org/stable/24939139>. Publisher: Scientific American, a division of Nature America, Inc.
- Jenkins, B. Hash functions. 1997.
- Johnston, I. *Exploration, Exploitation & Complexity in Biological Evolution and Self-Assembly*. doctoral thesis, University of Oxford, Oxford, UK, 2010.
- Johnston, I., Ahnert, S. E., Louis, A., and Doye, J. Evolutionary dynamics in a simple model of Self-Assembly. *Phys. Rev. E*, 2011. doi: 10.1103/PhysRevE.83.066105.
- Kumar, M., Husian, M., Upreti, N., and Gupta, D. GENETIC ALGORITHM: REVIEW AND APPLICATION. *International Journal of Information Technology and Knowledge Management*, 2(No. 2):451–454, December 2010.
- Langdon, W. Debugging CUDA. *GECCO'11*, 2011. doi: <http://delivery.acm.org/10.1145/2010000/2002028/p415-langdon.pdf>.
- Linden, D., Lohn, J., Hornby, G., and Kraus, W. Evolutionary design of an x-band antenna for NASA's space technology 5 mission. *Antennas and Propagation Society International Symposium, 2004. IEEE*, 3:2313 – 2316, 2004.

- M.A.Nowak. *Evolutionary Dynamics*. 2006.
- Matsumoto, M. and Nishimura, T. Mersenne twister: A 623-dimensionally equidistributed uniform pseudorandom number generator. *ACM Transactions on Modeling and Computer Simulation*, 8(1):3–30, January 1998.
- Mitchell, M. *A Introduction to Genetic Algorithms*. The MIT Press, 1998.
- Murthy, G. S., Ravishankar, M., Baskaran, M. M., and Sadayappan, P. Optimal loop unrolling for GPGPU programs. In *2010 IEEE International Symposium on Parallel Distributed Processing (IPDPS)*, pp. 1–11, April 2010. doi: 10.1109/IPDPS.2010.5470423. ISSN: 1530-2075.
- NVidia. PTX: parallel thread execution, October 2007. ISA Version 1.1.
- NVidia. Bioinformatics and life sciences (GPU), 2012a. URL http://www.nvidia.com/object/bio_info_life_sciences.html.
- NVidia. CUDA c best practices guide, January 2012b. URL http://developer.download.nvidia.com/compute/DevZone/docs/html/C/doc/CUDA_C_Best_Practices_Guide.pdf.
- NVidia. CUDA toolkit 4.1: CURAND guide, January 2012c. URL http://developer.download.nvidia.com/compute/DevZone/docs/html/CUDALibraries/doc/CURAND_Library.pdf.
- NVidia. CUDA c programming guide, 2012d. URL http://developer.download.nvidia.com/compute/DevZone/docs/html/C/doc/CUDA_C_Programming_Guide.pdf.
- Pedemonte, M., Alba, E., and Luna, F. Bitwise operations for GPU implementation of genetic algorithms. *Proceedings of the 13th annual conference companion on Genetic and evolutionary computation*, 2011. doi: 10.1145/2001858.2002031.
- Pospichal, P., Jaros, J., and Schwarz, J. Parallel genetic algorithm on the CUDA architecture. Brno, 2010. Masaryk University. ISBN 978-80-87342-10-7. URL http://www.fit.vutbr.cz/research/view_public.php?id=9432.
- Ronacher, A. Jinja2, 2012. URL <http://jinja.pocoo.org/docs/>.
- Rothmund, P. and Winfree, E. The program-size of self-assembled squares (extended abstract). 2000.
- Schatz, M., Trapnell, C., Delcher, A., and Varshney, A. High-throughput sequence alignment using graphics processing units. *BMC Bioinformatics*, (8):474, 2007. doi: 10.1186/1471-2105-8-474.
- Schmielau, T. t. Implementing a FIFO-list in shared memory using atomics, 2012. URL <https://forums.developer.nvidia.com/t/implementing-a-fifo-list-in-shared-memory-using-atomics-memory-inconsistencies-each-thread-in-a-wa/25864>.
- Shannon, C. A mathematical theory of communication. *Bell System Technical Journal*, 27:379–423, 1948.
- Soloveichik, D. and Winfree, E. Complexity of Self-Assembled shapes. *SIAM J. Comput.*, (36):1544–1569, 2007.
- Wagner, A. Robustness and evolvability: a paradox resolved. *Proceedings. Biological Sciences*, 275(1630): 91–100, January 2008. ISSN 0962-8452. doi: 10.1098/rspb.2007.1137.
- Wang, H. Proving theorems by pattern recognition — II. *The Bell System Technical Journal*, 40(1):1–41, January 1961. ISSN 0005-8580. doi: 10.1002/j.1538-7305.1961.tb03975.x. Conference Name: The Bell System Technical Journal.
- Whitesides, G. and Grzybowski, B. Self-Assembly at all scales. *Science*, 295:2418, 2002.
- Winfree, E., Liu, F., Wenzler, L., and Seeman, N. Design and Self-Assembly of two-dimensional DNA crystals. *Nature*, (394):539–544, 1988.
- Wright, S. The roles of mutation, inbreeding, crossbreeding and selection in evolution. *Proceedings of the XI International Congress of Genetics*, 8:209–222, 1932.
- Wu, N. Oxford haskell user group, 2012.

A. Classification of $S_{3,8}^{32}$

See Figures 12, 13, 14, 15, 16, 17, and 18.

B. Formalistic treatment of self-assembly

B.1. Winfree's abstract tile assembly model

Winfree's model extends planar self-assembly of Wang tiles (Rothemund & Winfree, 2000). A Wang tile T is a unit square with edges colored from a binding domain Σ (Wang, 1961). The binding domain Σ includes the neutral color null, which does not bond to any other color. A set of symmetric strength functions g indicates the interaction strengths between any two colors. Matching colors are assigned some positive integer value interaction strength, all other combinations are set to zero. Tiles may not be rotated nor flipped and there exists an empty tile which does not bond to any other tile. A *tileset* is the set of all tile types that may be used in the assembly process. Each tile type may be used arbitrarily often. A particular tile occupation pattern of the assembly plane is called a configuration. An individual step in the assembly process consists of randomly adding a further bonding tile from the tileset to the existing configuration. The free energy $G(C)$ of a configuration C is defined to be the sum over all interaction strengths between the assembled tiles (Rothemund & Winfree, 2000). The relative sizes of the free energy of a configuration and an abstract temperature \mathcal{T} determine whether a given assembly is temperature-stable, i.e. that it is fully connected and will not tend to dissociate into two or more smaller configurations over time. In general, if a tile T_i is added to an existing \mathcal{T} -stable configuration A , the resulting configuration B is \mathcal{T} -stable iff the sum over all bonding strengths to neighbour tiles of T_i is greater or equal to \mathcal{T} (Rothemund & Winfree, 2000). In order to fully specify a given assembly process, we need to specify a tile system $\mathbb{T} = \langle T, S, g, \mathcal{T} \rangle$. Here, T is a tileset including the *empty* tile and *Seed* is a set of *seed tiles* at specified positions, i.e. the initial configuration consists of *Seed* and empty tiles everywhere else. Each *tile system* \mathbb{T} has a map $\text{Prod}:\mathbb{T} \rightarrow \text{assembly configurations}$. The set $\text{Term}(\mathbb{T})$ is the subset of $\text{Prod}(\mathbb{T})$ which includes all configurations that *terminate* in finite time. If every possible assembly path through $\text{Prod}(\mathbb{T})$ results in an element of $\text{Term}(\mathbb{T})$ in finite time and the cardinality of $\text{Term}(\mathbb{T})$ is finite, then \mathbb{T} is said to be *halting*. (Rothemund & Winfree, 2000)

B.2. Modifications to Winfree's aTAM

Due to its two-dimensional nature, it has been suggested that abstract tile assembly model (aTAM) may be used to approximate self-assembly of proteins or protein sub-units on the surface of a planar substrate (Johnston et al., 2011, Fig. 1). In this light, Johnston et al. (2011) have suggested a modified version of aTAM, which I refer to as *JaTAM*. I now extend Winfree's *aTAM* formalism to Johnston's model. *JaTAM* fixes \mathcal{T} to the value of 1. This makes sense if building block interaction strengths are much larger than thermodynamic noise. The restriction $\mathcal{T} = 1$ means that for any configuration C , $G(C)$ is sufficiently large such that C is \mathcal{T} -stable. So g can be characterised by a binary matrix \mathcal{M} . *JaTAM* fixes \mathcal{M} to $M_{ij} = (1 - i \bmod 2)\delta_{i(j+1)} + (i \bmod 2)\delta_{i(j-1)}$, i.e. colors bond in adjacent pairs, which is in contrast to the color-matching scheme of *aTAM*. Adjacent pair-bonding may mimick the bonding scheme between complementary DNA bases. This *heterogeneous strength function* produces different phenomenology from *aTAM* (Ahnert et al., 2009). Johnston et al. (2011) allow orthogonal rotations of Wang tiles, such that each configuration additionally contains orientation flags of all assembled tiles. *Seed* is defined to be the first element in the tile set T , which is positioned at the center of an empty grid. Two configurations are equivalent iff all assembled tiles at each point of the assembly grid are equivalent in type and orientation. If the positions of all empty tiles coincide between two configurations, then they are *shape-equivalent* (Johnston, 2010). A given \mathbb{T} is deterministic iff all assembly paths through $\text{Prod}(\mathbb{T})$ terminate in equivalent configurations. Otherwise, \mathbb{T} is *non-deterministic*. Iff a given configuration A contains non-empty tiles at positions outside an origin-centred square of dimension d , then A is said to be unbounded by d . Otherwise, A is bounded by d . Iff \mathbb{T} is halting, then we can always find a finite, positive z such that $\text{Prod}(\mathbb{T})$ is bounded by z . Let the *assembly frontier* be the set of all assembly grid positions that are occupied by an empty tile and have at least one non-empty neighbour tile. Let's choose some *non-deterministic* \mathbb{T}^* . For any configuration $A \in \text{Prod}(\mathbb{T}^*)$, let B denote the set of configurations generated after one further tile α has been assembled on the assembly frontier of A . Let P be the point where tile α has been assembled. If B contains a subset of configurations which correspond to equal P but are not all equivalent to each other, then \mathbb{T}^* is said to exhibit trivial non-determinism. *Steric non-determinism* arises if at least two partial assembly paths exclude each other without the involvement of trivial non-determinism. Phenomenologically, this arises when two or more independently growing "arms" converge (Johnston, 2010). \mathbb{T}^* may exhibit trivial non-determinism and steric non-determinism at the same time. I now proceed by extending Johnston's terminology by defining a shape-similarity measure. I define the shape-difference

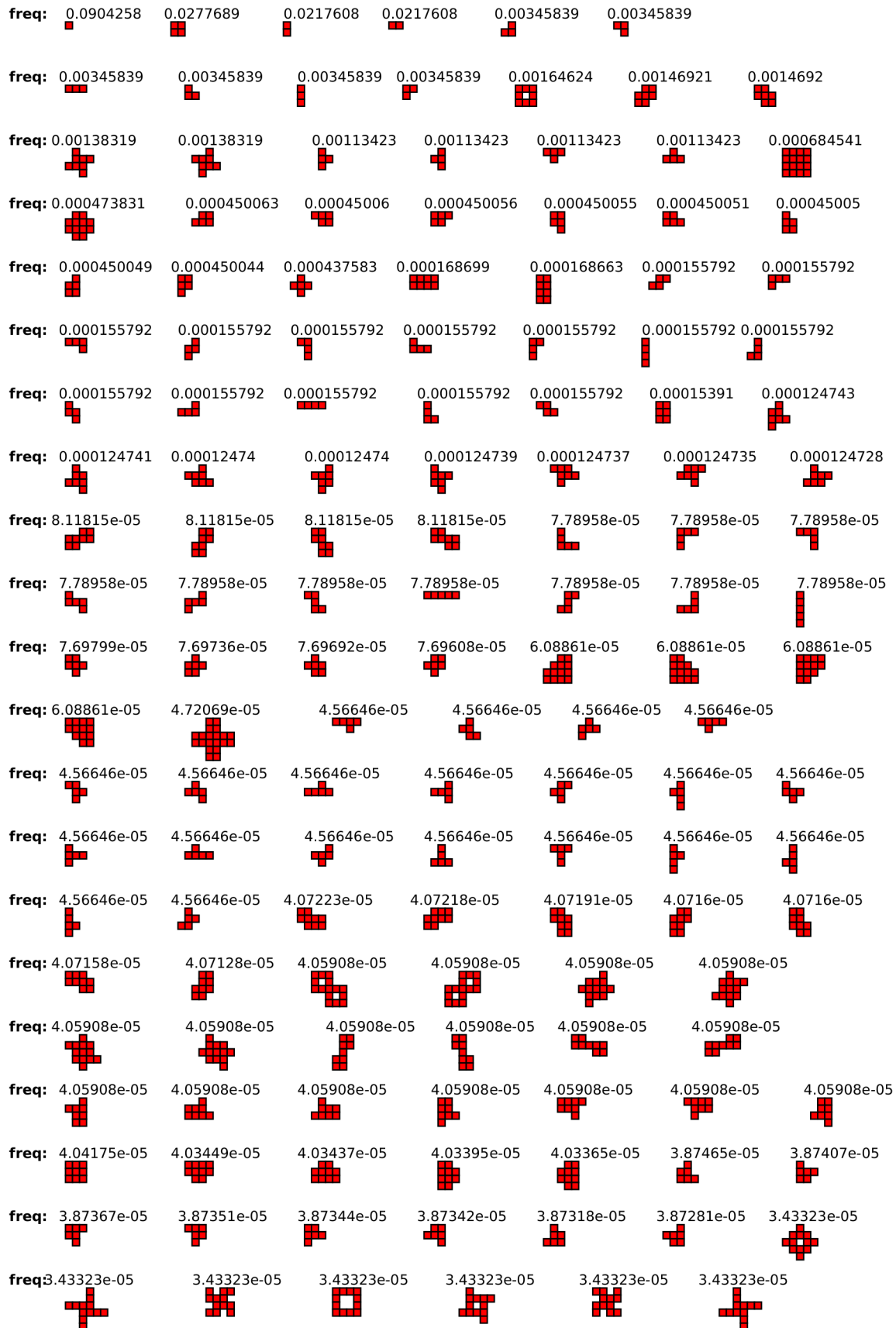


Figure 12. [1] Classification of $S_{3,8}^{32}$ at 7 redundancy assemblies for detection of steric nondeterminism, ordered by frequency. Frequencies are calculated with respect to the whole genome search space of size 2^{32} .

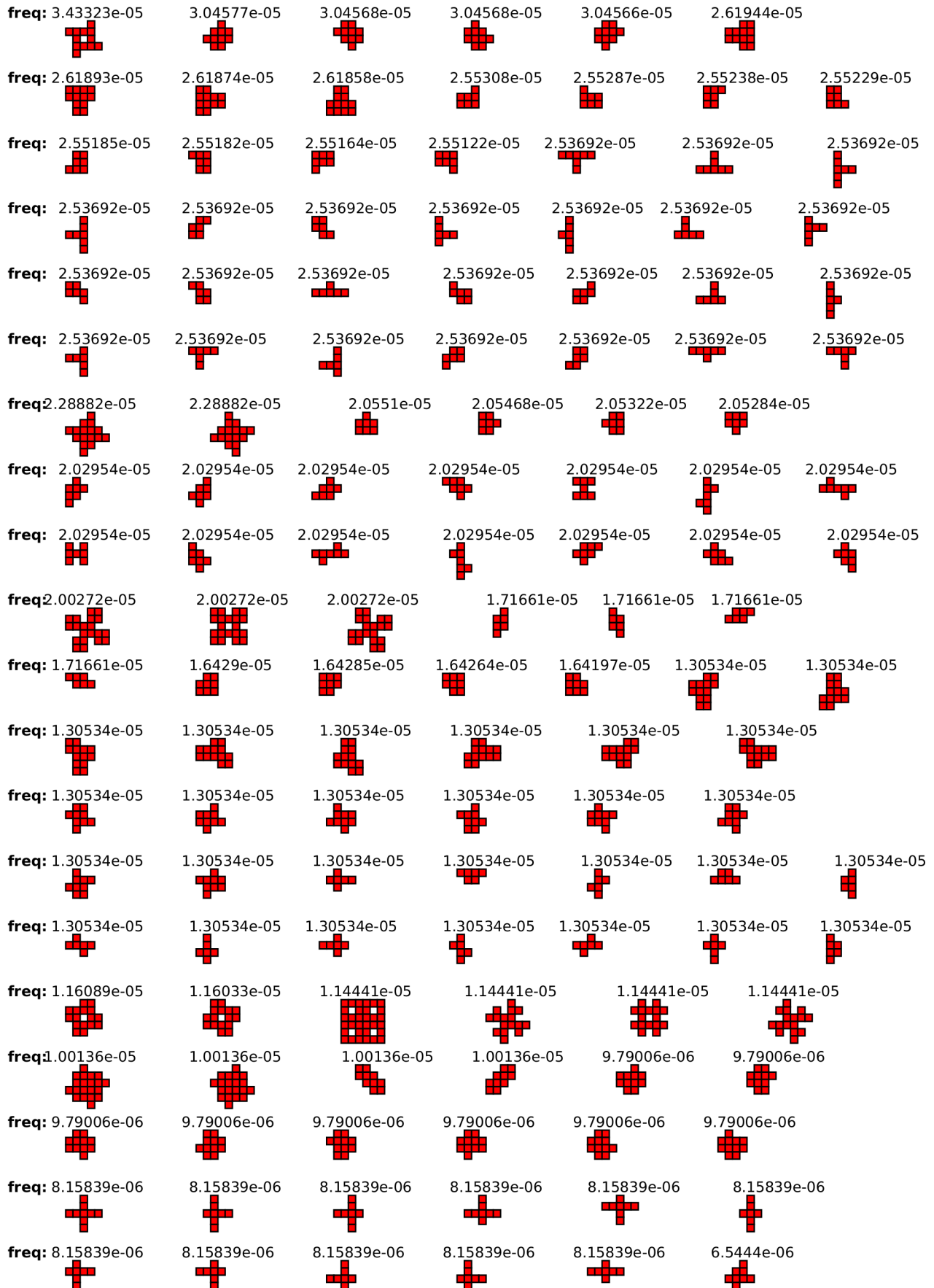


Figure 13. [2] Classification of $S_{3,8}^{32}$ at 7 redundancy assemblies for detection of steric nondeterminism, ordered by frequency. Frequencies are calculated with respect to the whole genome search space of size 2^{32} .

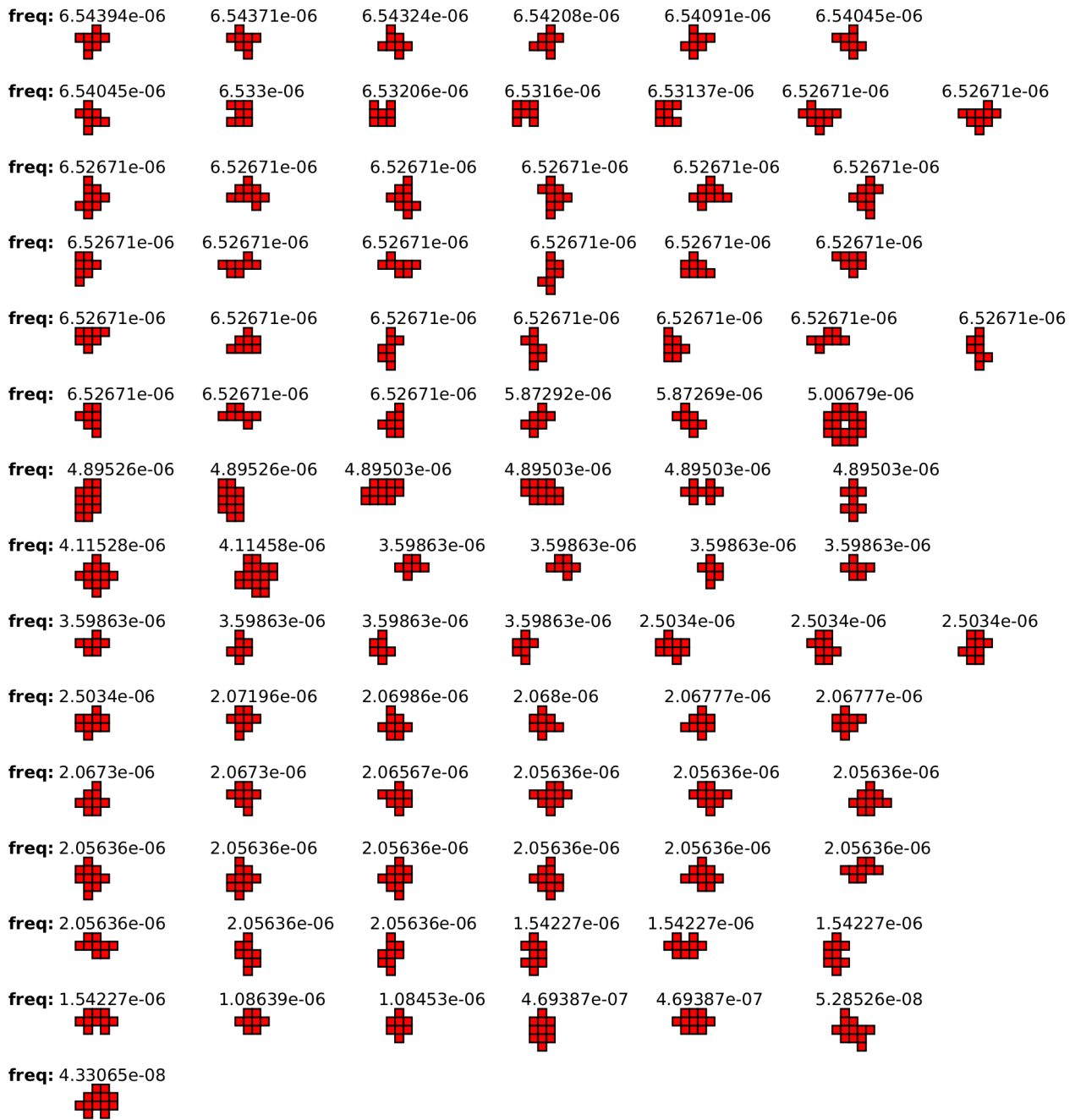


Figure 14. [3] Classification of $S_{3,8}^{32}$ at 7 redundancy assemblies for detection of steric nondeterminism, ordered by frequency. Frequencies are calculated with respect to the whole genome search space of size 2^{32} .

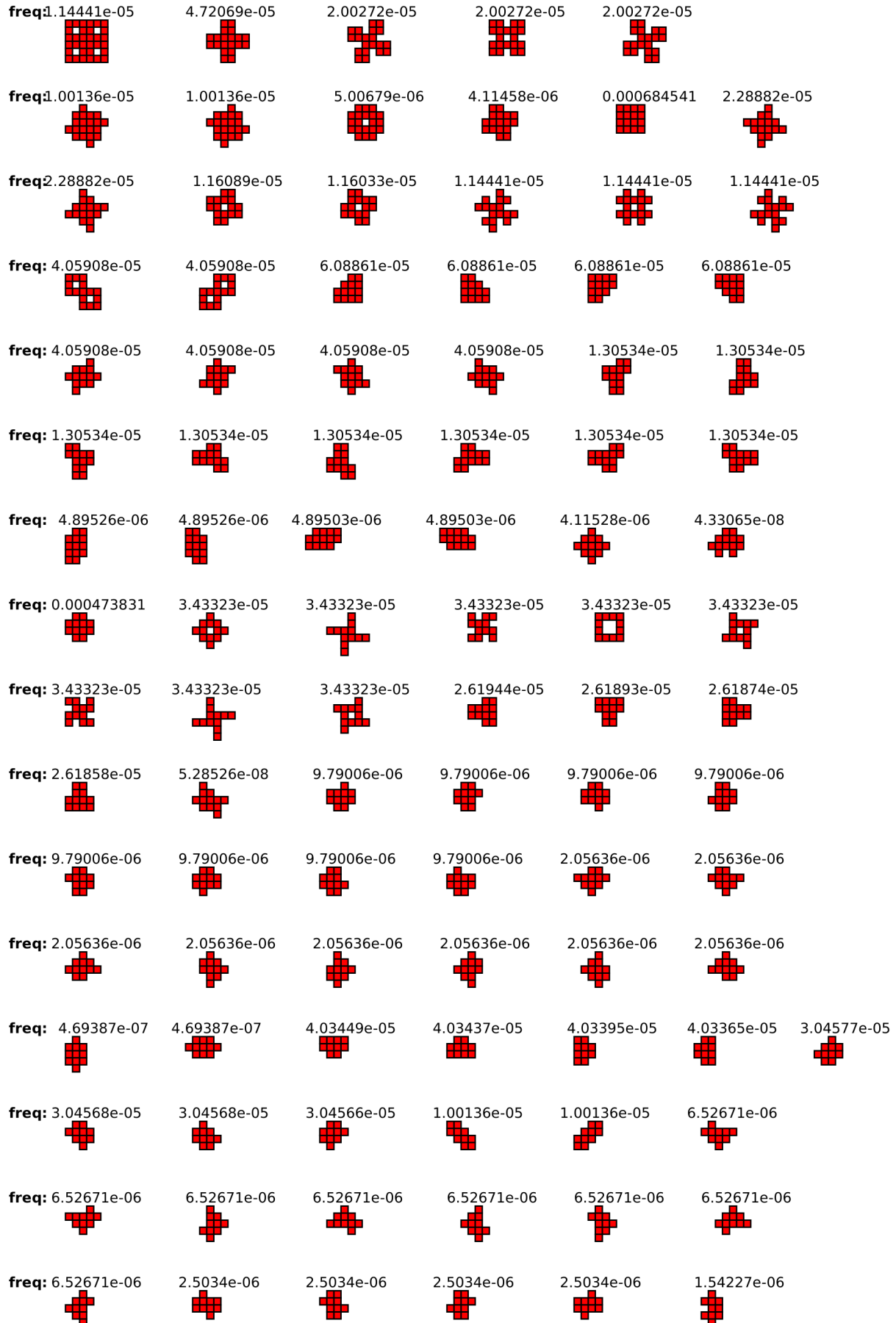


Figure 15. [4] Classification of $S_{3,8}^{32}$ at 7 redundancy assemblies for detection of steric nondeterminism, ordered by frequency. Frequencies are calculated with respect to the whole genome search space of size 2^{32} .



Figure 16. [5] Classification of $S_{3,8}^{32}$ at 7 redundancy assemblies for detection of steric nondeterminism, ordered by frequency. Frequencies are calculated with respect to the whole genome search space of size 2^{32} .



Figure 17. [6] Classification of $S_{3,8}^{32}$ at 7 redundancy assemblies for detection of steric nondeterminism, ordered by frequency. Frequencies are calculated with respect to the whole genome search space of size 2^{32} .



Figure 18. [7] Classification of $S_{3,8}^{32}$ at 7 redundancy assemblies for detection of steric nondeterminism, ordered by frequency. Frequencies are calculated with respect to the whole genome search space of size 2^{32} .

shapediff(A, B) $\in \mathbb{N}$ of two configurations A, B to be the number of non-coinciding empty tile positions between A and B . Then, iff A, B are just bounded by d , the shape-similarity $\text{shapesim}(A, B) \in [0, 1]$ of A, B is defined to be equivalent to $1 - \text{shapediff}(A, B)/d^2$. As tile-shaped building blocks may bind to a substrate from either above or below, and Johnston et al. (2011) suggest a future assembly-system, which allows tiles bonding from two sides to be arbitrarily flipped in the substrate plane. In this paper, however, I will restrict myself to JaTAM, which is reasonable if we assume that tiles only bind to the substrate from a single side.

B.3. Encoding genome information

By Shannon (Shannon, 1948), in order to label $|\mathcal{G}_D|$ genome microstates, an average number of $\log_2|\mathcal{G}_D|$ bits are needed. While, in principle, we are free to choose any such encoding, there are particular choices of binary encodings that are more natural than others based on characteristics of the evolutionary operators acting on the search space S . These characteristics should be equivalent to their counterparts in natural DNA encoding.

Applying a suitable mutation operator \mathfrak{M} to some genome $G \in S$ needs to yield another element $\in S$. A formal way of stating this is to say that S is closed under the operator \mathfrak{M} . Furthermore, any $X \in S$ must be transformable into any arbitrary element $\in S$ with non-zero probability in a finite number of steps, i.e. \mathfrak{M} is *permuting*. A suitable single-point crossover operator \mathfrak{C} needs to be such that S is closed under it as well. However, it is not a permuting operator, which can be seen by choosing two genomes with uniform base occupations - however often we recombine the two, we will never be able to create a permutation that contains the third or fourth base type used by DNA encoding. A characteristic property of \mathfrak{C} is, however, that it preserves the relative order of all genes involved.

I conclude that with respect to mutation, the choice of what bases constitute a particular gene is arbitrary. For *single-point crossover*, however, relative order of genes has to be preserved and this can in the general case only be defined if all bases belonging to a particular gene sit at adjacent locations in the genome. The observation of genetic drift, however, strongly depends on the correlation between a particular gene and its phenotypic expression. Whether it is possible to define a gene-interpretation for Johnston's model that allows for strong correlations between genotypes and phenotypes is a key question for further research. *Kolmogorov complexity* $\mathcal{K}(s_b)$ is defined as the shortest program size written in a language \mathbb{L} which can output a bitstring s_b . We will in the following define \mathbb{L} to be the language of a *Universal Turing Machine*. A phenotype shape in aTAM can be defined by supplying a list of the locations of all non-empty tiles, which I call a list representation of that shape. Winfree et al. (1988) showed that \mathcal{K} of the list representation of a scale-free phenotype shape is proportional to the minimum number n of tile types, with respect to some tile system \mathbb{T} , that *deterministically* assembles that shape (Soloveichik & Winfree, 2007). Even though the relationship to \mathcal{K} of heterogeneous strength functions is not strictly proven (Soloveichik & Winfree, 2007), Ahnert et al. (2009) provide an algorithm which computes n with respect to a phenotype shape assembled by JaTAM and is of the same order as the respective Kolmogorov complexity (Ahnert et al., 2009). With respect to JaTAM, I conclude that a strongly phenotype-correlated gene-interpretation might consist of gene 1 being the minimum number of tile types required to compute the phenotype shape encoded in the genome and a gene 2 which encodes a notion of shapescala. Such an encoding does not exclude a constant bitstring binary encoding with respect to M . Defining the action of the operator \mathfrak{C} on such a binary encoding, however, is non-trivial and subject to further research.

I finally describe the constant bitstring binary encoding used by Johnston et al. (2011) and how the respective action of \mathfrak{M} may be defined. Johnston encodes a general tile set in the genome by sequentially encoding each tile in the tile set to a bitstring, starting with the seed tile. This is achieved by subsequently encoding all four colors of the tile in the order north-east-southwest, as looking down on the configuration grid. The number of bits required to encode a particular color is $\log_2\|\Sigma\|$ and Johnston always minimises the number of bits required. The action of \mathfrak{M} on this representation of S is to flip a number $n\mu$ of distinct bits, where $n\mu$ is Poisson-distributed with mean μ . As this implies a non-zero probability for the flipping of just a single bit, sequential \mathfrak{M} -operations can be used to traverse arbitrary Hamming weight distances in search space and \mathfrak{M} is thus permuting. To achieve closure under \mathfrak{M} , I conclude that Johnston's encoding restricts $\|\Sigma\|$ to integer powers of 2. It is now trivial to define the map tileset, which decodes Johnston's binary encoding into a tileset.

C. On Flow Charts, Unit Tests and UML diagrams

In many situations, flow charts are an insightful way to represent the procedural large-scale flow of a program. In order to turn a piece of code into a flow chart, one first represents all branches and loops as an empty flow-chart and then fills in the pictograms with some short-hand summary of the action of the underlying code. The content of each pictogram then defines

a particular code unit. The functionality of each code unit may be described by the help of abstract pseudo code. In order to ensure the integrity of a code unit, a carefully-written unit test should be designed. A unit test defines a set of input values to a code unit and specifies the desired set of output values. The distribution of input values can be a random distribution or tailored to test particularly suspicious parameter ranges. The assertion strength of a unit test is thus dependent on the choice of input values. A principal advantage of unit tests is that they can act on black boxes, i.e. program parts whose precise internals that cannot or should not be presented to a general audience. By publishing the input parameters of the unit test, however, and the resulting output parameters, one can display code integrity without the need of detailed code disclosure or analysis. Furthermore, large and complex code units may be broken down into simpler, independent components which can be unit-tested individually. If a piece of software is designed in an object-oriented way, flow charts may be replaced by Unified-Modeling language (UML) diagrams. UML is a very broad standard allowing the graphical representation of flow processes in a large number of domains. A particular type of UML diagram is a class diagram which represents all classes, their attributes and their relationships with each other. There exist tools that can generate UML class diagrams from source code and also some that allow the generation of source code from such a diagram.

C.1. Tournament Selection in Haskell

In order to illustrate how functional programming is independent of program flow, I attach snippets in **C** and **Haskell** used for tournament selection: We supply a list of weights and a cut-off index (which is usually chosen randomly) and would like our function to return the counter index of the element where the sum of the weights is greater or equal to the cut-off index.

C.1.1. C-IMPLEMENTATION

```
unsigned int tourn(void) {
    for(int i=0;i<mWeightLen;i++){
        partsum += weights[i];
        if(partsum >= cutoff){
            counter = i;
            break;
        }
    }
    return counter;
}
```

We initialise *global* parameters as follows:

```
#define mWeightLen 4
float weights[mWeightLen] = {2.0,3.0,4.0,1.0}
unsigned int cutoff = 10;
unsigned int counter = 0;
float partsum = 0.0f;
```

C.1.2. HASKELL-IMPLEMENTATION

```
tourn :: [Double] -> [Integer] -> Double -> Double -> Integer
tourn (x:xs) (y:ys) z p = if (p+x) >= z then y else tourn xs ys z (p+x)
```

The parameters should be initialised as follows:

```
weights = [2.0,3.0,4.0,1.0]
indices = [0.. fromIntegral (length weights)]
cutoff = 10.0
counter = 0.0
```

We note that *tourn* is simply a *curried, recursive* function. The internal flow of this function is determined by the *compiler* only.

D. Efficient bit-wise implementations of common evolutionary operators

D.1. Mutation from Poisson Distribution

An implementation of mutation from Poisson distribution follows below. Note that we could reduce the required storage space for the bitmask, of course at the expense increasing computing time, by using a dynamic list to keep track of the flipped bits. Dynamic lists in *shared memory*, however cannot be efficiently implemented as there is no *heap* available.

```

__forceinline__ __device__ void ga_MutationSophisticated( unsigned char (&s_ucGenome)
                                                         [m_ga_NR_THREADS_PER_BLOCK][mByteLengthGenome],
                                                         unsigned char (&s_ucBufGenome)
                                                         [m_ga_NR_THREADS_PER_BLOCK][mByteLengthGenome],
                                                         float mutation_rate,
                                                         curandState *state){
    for(int i=0;i<mByteLengthGenome;i++){
        s_ucBufGenome[mTHREAD_ID][i] = 0;
    }
    float r_fNrMutations = ga_uiPoissonDistribution(mutation_rate, state);
    if(r_fNrMutations > mBitLengthGenome) r_fNrMutations = mBitLengthGenome;
    float r_fRandBuf;
    short r_ssBitOffset, r_ssByteOffset;
    bool r_bRetry = false;
    for(int i=0;i<r_fNrMutations;i++){
        r_fRandBuf = curand_uniform(state) * mBitLengthGenome;
        r_ssBitOffset = (signed short) r_fRandBuf % 8 ;
        r_ssByteOffset = ((signed short) r_fRandBuf - r_ssBitOffset) / 8;
        if( ! ( s_ucBufGenome[mTHREAD_ID][r_ssByteOffset] & (1 << r_ssBitOffset))){
            s_ucBufGenome[mTHREAD_ID][r_ssByteOffset] += (1 << r_ssBitOffset);
            r_bRetry=false;
        } else {
            i--; //Try again to mutate!
        }
    }
    for(int i=0;i<mByteLengthGenome;i++){
        s_ucGenome[mTHREAD_ID][i] = mXOR(s_ucGenome[mTHREAD_ID][i],
        s_ucBufGenome[mTHREAD_ID][i]);
    }
}

```

D.2. Single-point crossover

An efficient implementation of *single-point crossover*, which uses byte-wise operations instead of bit-wise operations. A further performance gain would be achieved by further increasing the granularity using *reinterpret_cast* as the *genome bytelength* exceeds a couple of bytes (up to 8 for double precision).

```

__forceinline__ __device__ void ga_CrossoverSinglePoint(unsigned char (&s_ucGenome)
                                                         [m_ga_NR_THREADS_PER_BLOCK]
                                                         [mByteLengthGenome],
                                                         unsigned char *g_ucGenomes,
                                                         unsigned int r_uiCutoffIndex,
                                                         curandState *state){
    unsigned short int r_uiCrossoverPoint = curand_uniform(state) * mBitLengthGenome;
    unsigned short int r_uiCrossoverBitOffset = r_uiCrossoverPoint % 8;
    unsigned short int r_uiCrossoverByte =
        (r_uiCrossoverPoint - r_uiCrossoverBitOffset) / 8;
}

```

```

unsigned int r_uiIndexBuffer;
for (int j=0; j<=r_uiCrossoverByte; j++){
    if (j == r_uiCrossoverByte){
        s_ucGenome[mTHREAD_ID][j] = ( s_ucGenome[mTHREAD_ID][j]
            & ( 0xFF >> r_uiCrossoverBitOffset ) )
            + ( g_ucGenomes[r_uiCutoffIndex * mByteLengthGenome + j]
            & ( 0xFF << ( 8 - r_uiCrossoverBitOffset ) ) );
    } else {
        s_ucGenome[mTHREAD_ID][j] =
            g_ucGenomes[r_uiCutoffIndex * mByteLengthGenome + j];
    }
}
}

```

D.3. Uniform crossover

An efficient implementation of uniform crossover, where both genomes are randomly interleaved on bit-level. Note that interleaving occurs in multiples of 4 bytes, which is the number of bytes that a call to the random number function generates.

```

__forceinline__ __device__ void ga_CrossoverUniform(unsigned char (&s_ucGenome)
    [m_ga_NR_THREADS_PER_BLOCK]
    [mByteLengthGenome],
    unsigned char *g_ucGenomes,
    unsigned int r_uiCutoffIndex,
    curandState *state ){
    unsigned int r_uiNumberOfRandCallsRequired = (unsigned int)
        ((mByteLengthGenome - mByteLengthGenome%sizeof(float))/sizeof(float) + 1);
    float r_fRandBuffer;
    unsigned char r_ucRandMask;
    unsigned int r_uiIndexBuffer;
    for (int i=0; i<r_uiNumberOfRandCallsRequired; i++){
        r_fRandBuffer = curand_uniform(state);
        for (int j=0; j<sizeof(float); j++){
            r_ucRandMask = (unsigned int) ((reinterpret_cast<int&>(r_fRandBuffer)
                & (0xFF << 8 * j)) >> 8 * j);
            r_uiIndexBuffer = i*sizeof(float) + j;
            if (r_uiIndexBuffer < mByteLengthGenome){
                s_ucGenome[mTHREAD_ID][r_uiIndexBuffer] = (s_ucGenome[mTHREAD_ID]
                    [r_uiIndexBuffer] & r_ucRandMask) + (g_ucGenomes
                    [ga_xGlobalAnchor(r_uiCutoffIndex * mByteLengthGenome +
                    r_uiIndexBuffer)] & (~r_ucRandMask)) ;
            }
        }
    }
}

```

E. PyCUDA - tips and tricks

This section includes some work-arounds which I needed to employ in order to get things work and which I could not find in any forum or document.

E.1. Getting *curand* to work

PyCUDA is designed such that python code can call kernel functions defined in *C/C++*. For this purpose, it requires knowledge of the exact reference name of the function used by the compiler. In *C*, this is merely the name of the function as

defined by the programmer. C++, however, supports functions of equal naming but different *namespaces*. In order to keep track of these functions, the compiler *name-mangles* them to some label unpredictable to *PyCUDA*. As *curand_kernel*-header uses different *namespaces*, it requires name-mangling to be activated, while the rest of the kernel code may not feature it. This problem may be solved by setting the Source Module-Option ‘no_extern_c’ to ‘True’ and enclosing everything but the header in *extern ‘C’*-brackets.

E.2. Unrolling for-loops using meta-templating

Interestingly, unrolling small for-loops may result in performance gains of up to a factor of 2, as has been observed previously (Murthy et al., 2010). An automatised way of unrolling loops at runtime is the usage of a metatemplating language, such as *Jinja2*(Ronacher, 2012). The following code segment demonstrates the *A*-times unrolling of a loop:

```
{% for idx in range(A) %}
    this->data.flags[__xThreadInfo.BankId()].set_Red({{ idx }});
    this->Assemble_Movelist(__xThreadInfo, __xGenomeSet);
    __syncthreads();
{% endfor %}
```

F. Selected Algorithms

F.1. Bit operations and casting

Using genome bit-representation instead of e.g. **boolean** representation allows the usage of very fast bit-operations which directly translate into x86 processor instructions. For reference, I include basic usage of bit operations on the *n*th bit in C/C++:

Bit setting

```
genome |= (1 << n);
```

Bit clearing

```
genome &= ~(1 << n);
```

Bit testing

```
genome & (1 << n);
```

Bit toggling

```
genome ^= (1 << n);
```

Modulo 2 operations

```
n%2 == n & 0x1;
```

All these operations can be effectively parallelised for a larger number of bits using *bitmasks*.

F.2. The use of `reinterpret_cast`

The data type of a memory segment may be re-interpreted as a different data type by the usage of either *unions* in C and */* or *reinterpret_cast* in C++. With caution, pointers reinterpreted by *reinterpret_cast* may be de-referenced. In this way, char-arrays may be initialised with a step length of up to 16-byte on GPU, which I found to be about 4 times faster than char-wise initialisation. For *gcc*-based compilers (such as likely *nvcc*), dereferencing a reinterpreted pointer may trigger the following warning: warning: type punned pointer will break strict-aliasing rules. This warning can be eliminated by setting the flag *-fno-strict-aliasing*. This does take away some optimisation options from the compiler, however, from my experience is usually acceptable performance-wise.

F.3. Bit operations and casting in Python

As python does not natively implement fixed-size numeric datatypes, the usage of bit operations may not be as performant as for C/C++. However, equivalent operators may be used e.g. for calculating *Jenkin's hash* (Jenkins, 1997). The size of the data type may then be selected afterwards using a bitmask (i.e. to select a 32-bit data type from a pythonic number x , we may use $x \&= 0xffffffff$ to set higher bits to zero.) As python does not offer pointer manipulation natively, one needs to employ a foreign-function interface such as *ctypes* in order to implement C/C++-style union data types and/or type casting.

F.4. One-at-a-time Hash

The following is an efficient implementation of a 32-bit hash function taking one byte at a time by Jenkins (Jenkins, 1997). This so called One-at-a-time hash has a decent avalanche behaviour and is very fast.

```

__device__ void jenkins_init(int &hash){
    hash = 0;
}
__device__ void jenkins_add(char key, int &hash){
    unsigned int tmphash=hash;
    tmphash += key;
    tmphash += (tmphash << 10);
    tmphash ^= (tmphash >> 6);
    hash=tmphash;
}
__device__ unsigned int jenkins_clean_up(int &hash){
    unsigned int tmphash=hash;
    tmphash += (tmphash << 3);
    tmphash ^= (tmphash >> 11);
    tmphash += (tmphash << 15);
    hash = tmphash;
    return hash;
}
    
```

F.5. Reentrant LIFO-Stack

I thank *tera* (Schmielau, 2012) for making me aware of undercurrent and overcurrent detection issues arising from the use of atomic operations in *CUDA* with unsigned data types. The following is a push-function, designed by *tera*, which has been made multi-threading safe for use in a multi-threaded *LIFO*-stack implementation:

```

__device__ bool x_push(int entry, unsigned int *pos_p, int max_length, int* stor){
    unsigned int BankID = threadIdx.x % 32;
    unsigned int pos = atomicAdd(pos_p, 1);
    if(pos < max_length){
        stor[BankID + pos*32] = entry;
        return true;
    } else {
        atomicSub(pos_p, 1);
        return false;
    }
}
    
```

Note: *pos_p* should be initialised to 0. Note also that changes in the usage of atomic functions which would be valid for *boost* threads may readily lead to data inconsistencies for usage with *CUDA*.

F.6. Parallelised grid cropping

The following parallelised code determines the upper left and the lower right crop corner of an assembly grid:


```

if(__xThreadInfo.WarpId()==0){
    this->data.corner_lower[__xThreadInfo.BankId()]=make_int2(0,0);
    this->data.corner_upper[__xThreadInfo.BankId()]=
        make_int2(m_fit_DimGridX-1, m_fit_DimGridY-1);
    this->data.assembly_size[__xThreadInfo.BankId()]=0;
}
__syncthreads();
short offset = (m_fit_DimGridX*m_fit_DimGridY) % mBankSize;
short myshare = (m_fit_DimGridX*m_fit_DimGridY - offset) / mBankSize;
int off_x=0, off_y=0;
for(int i=0;i<myshare;i++){
    off_x = (myshare*__xThreadInfo.WarpId()+i) % m_fit_DimGridX;
    off_y = (myshare*__xThreadInfo.WarpId()+i-off_x) / m_fit_DimGridX;
    if(this->data.grid.data.multi_d[off_x][off_y][this->data.flags
        [__xThreadInfo.BankId()].get_ucRed()]
        [__xThreadInfo.BankId()].get_xCell()!=mEMPTY_CELL){
        atomicMin(&this->data.corner_upper[__xThreadInfo.BankId()].x, off_x);
        atomicMin(&this->data.corner_upper[__xThreadInfo.BankId()].y, off_y);
        atomicMax(&this->data.corner_lower[__xThreadInfo.BankId()].x, off_x);
        atomicMax(&this->data.corner_lower[__xThreadInfo.BankId()].y, off_y);
    }
}
if(__xThreadInfo.WarpId()==mBankSize-1){
    for(int i=0;i<offset;i++){
        if(this->data.grid.data.multi_d[off_x][off_y]
            [this->data.flags[__xThreadInfo.BankId()].get_ucRed()]
            [__xThreadInfo.BankId()].get_xCell()!=mEMPTY_CELL){
            atomicMin(&this->data.corner_upper[__xThreadInfo.BankId()].x, off_x);
            atomicMin(&this->data.corner_upper[__xThreadInfo.BankId()].y, off_y);
            atomicMax(&this->data.corner_lower[__xThreadInfo.BankId()].x, off_x);
            atomicMax(&this->data.corner_lower[__xThreadInfo.BankId()].y, off_y);
        }
    }
}
}

```

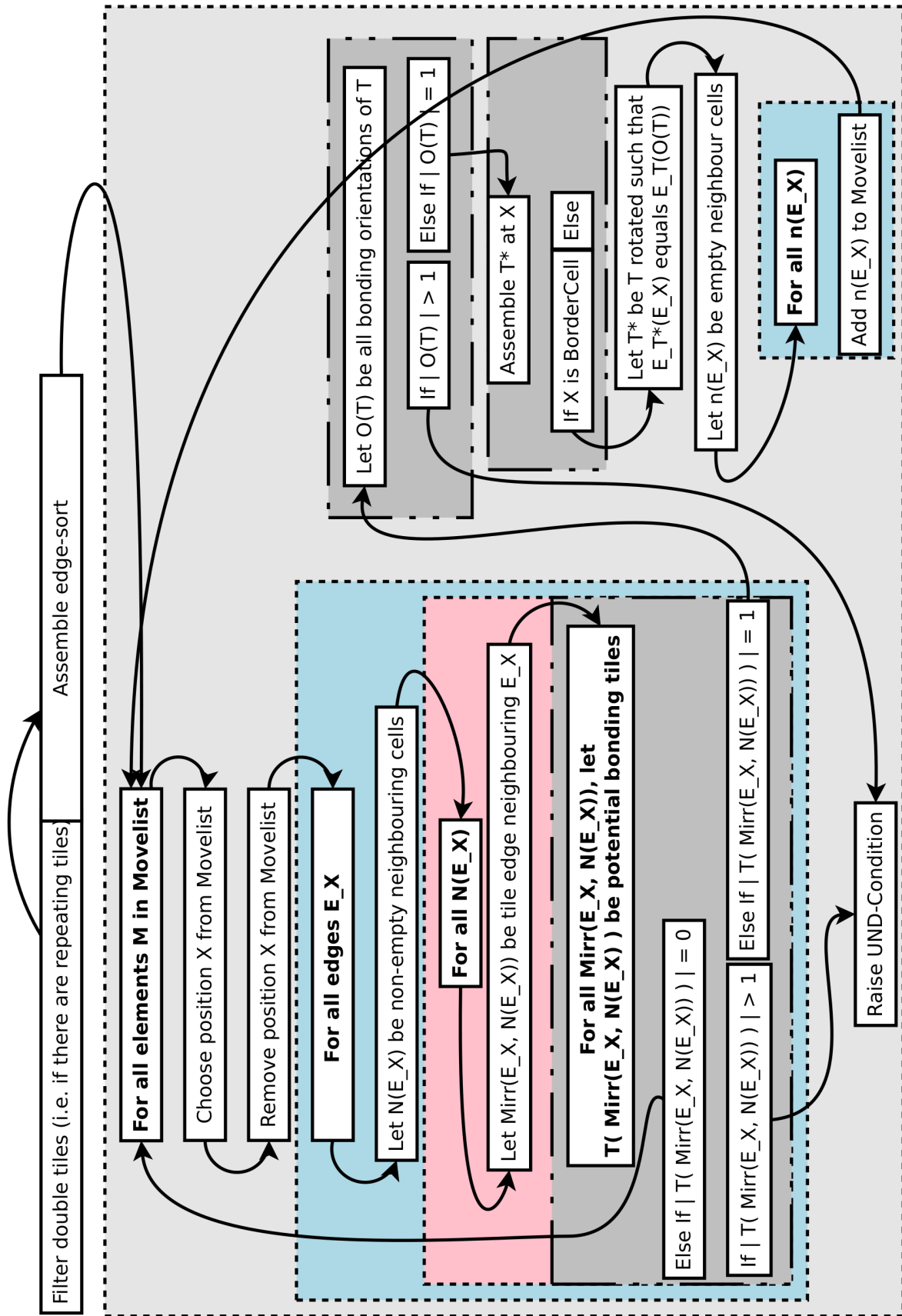


Table 1. A simplified set-theory inspired flow chart for the movelist polyomino assembly algorithm used in this paper.

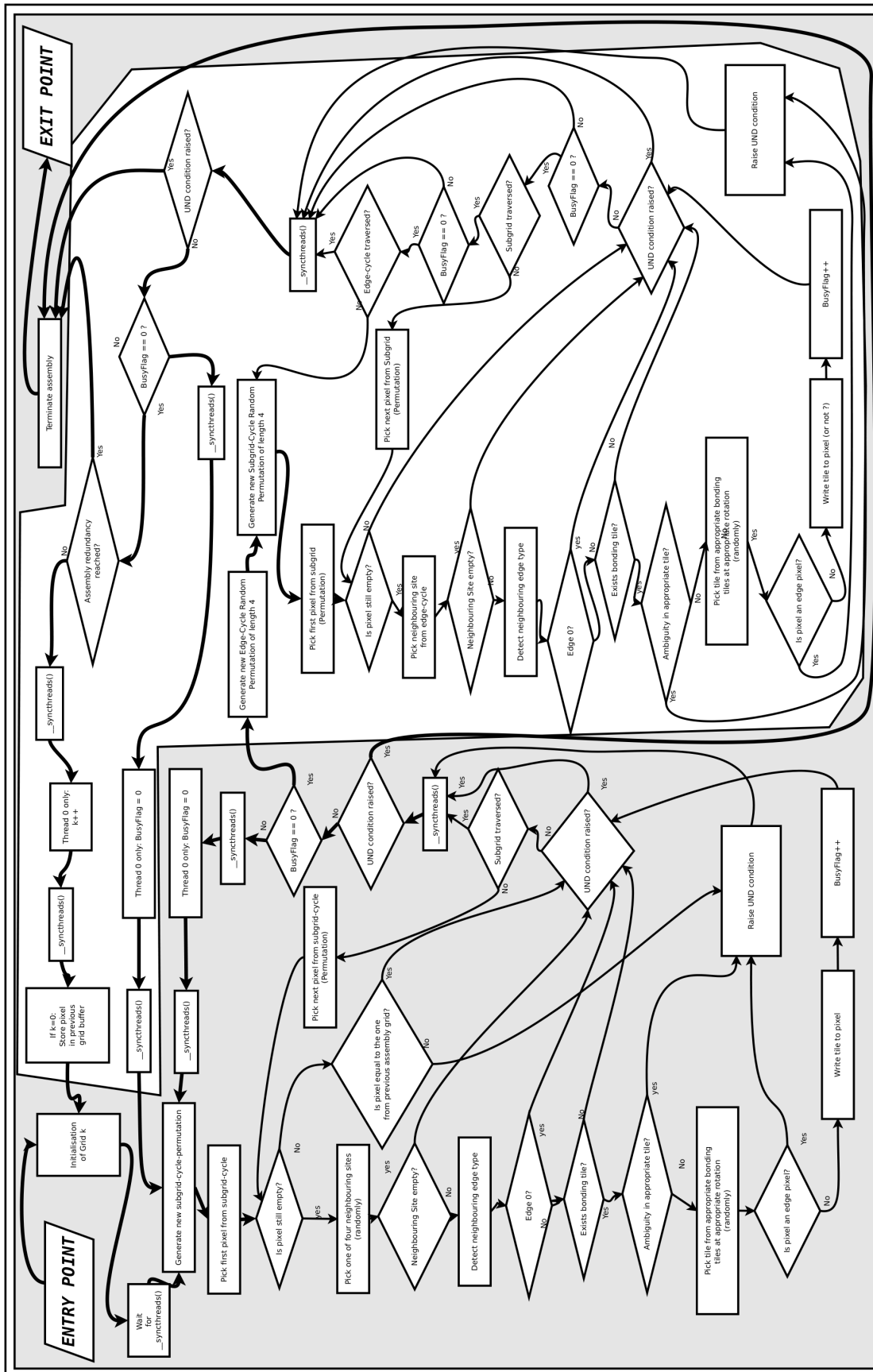


Table 2. An optimised flow chart for an in-place polyomino assembly algorithms which could be used to take over in case that movelist storage does not suffice.

